UV Photo-dissociation of proline-containing peptide ions: Insights from molecular dynamics

Marion Girod, Zeljka Sanader, Marin Vojkovic, Rodolphe Antoine, Luke Macaleese, Jérôme Lemoine, Vlasta Bonacic-Koutecky, Philippe Dugourd

UV Photo-dissociation of proline-containing peptide ions: Insights from molecular dynamics

Marion Girod[a, b*], *Zeljka Sanader*[c], *Marin Vojkovic*[a, d], *Rodolphe Antoine*[a, d], *Luke MacAleese*[a, d], *Jérôme Lemoine*[a,b], *Vlasta Bonacic-Koutecky*[c,e] *and Philippe Dugourd*[a,d*]

[a] Université de Lyon, F-69622, Lyon, France ;

[b] CNRS et Université Lyon 1 UMR 5280, Institut des Sciences Analytiques

[c] Interdisciplinary Center for Advanced Science and Technology (ICAST) at University of Split, Split, Croatia

[d] CNRS et Université Lyon 1, UMR5306, Institut Lumière Matière

[e] Humboldt-Universität Berlin, Institut fur Chemie, Berlin, Germany

[*]**To whom correspondence should be addressed:**

Philippe Dugourd: philippe.dugourd@univ-lyon1.fr

Marion Girod: marion.girod@univ-lyon1.fr

Running title: photodissociation of proline peptides.

ABSTRACT

UV photodissociation of proline-containing peptide ions leads to unusual product ions. In this paper, we report laser-induced dissociation of a series of proline-containing peptides at 213 nm. We observe specific fragmentation pathways corresponding to the formation of (y-2), (a+2) and (b+2) fragment ions. This was not observed at 266 nm or for peptides which do not contain proline residues. In order to obtain insights into the fragmentation dynamics at 213 nm, a small peptide (RPK for arginine-proline-lysine) was studied both theoretically and experimentally. Calculations of absorption spectra and non-adiabatic molecular dynamics (MD) were made. Second and third excited singlet states, S_2 and S_3, lie close to 213 nm. Non-adiabatic MD simulation starting from S_2 and S_3 shows that these transitions are followed by C-C and C-N bond activation close to the proline residue. After this first relaxation step, consecutive rearrangements and proton transfers are required to produce unusual (y-2), (a+2) and (b+2) fragment ions. These fragmentation mechanisms were confirmed by H/D exchange experiments.

Keywords

Laser induced dissociation; proline-containing peptides; fragmentation; molecular dynamics; H/D exchange

Introduction

Tandem mass spectrometry (MS/MS) is a widely-used method to determine the amino acid sequence of peptides and proteins [1]. In addition, the use of CID (collision-induced dissociation) continues to be important in peptide sequencing and protein identification. In solution, the most basic site on a peptide devoid of histidine, lysine, and arginine residues is the nitrogen atom of the N-terminal amino group [2]. However, once the protonated peptide ion is desorbed into the gas phase, e.g. via electrospray, there is competitive transfer of the "ionizing" proton to amidic functional groups, the carbonyl oxygen and amidic nitrogen atoms on the backbone [3-8]. The peptide then fragments at the protonated peptide bond [9, 10]. A non-terminal residue has two adjacent peptide linkages, one to the N-terminal and the other to the C-terminal. At low (<100 eV) energy CID, the protonated peptides fragment along the backbone at the amide bonds, and the mass spectrum typically consists of a series of *b*, *a*, and *y* fragment ions. These fragments give valuable information [9, 10] concerning peptide sequence, number and location of disulfide bridges, identification and sometimes characterization of post-translational modifications. However, fragmentation pathways of protonated peptides are difficult to understand and known only at the phenomenological level.

It is apparent from the diverse CID patterns observed that the fragmentation routes of protonated peptides depend significantly on the identity and positions of the amino acids constituting the peptides. It was found that proline (Pro) and to a smaller extent glycine and serine residues tend to fragment at their N-terminal peptide bonds, whereas residues such as valine and isoleucine tend to fragment toward their C-terminal peptide bonds [11]. Other published work using tandem MS on peptides, e.g., ubiquitin, have often indicated unusually abundant product ions resulting from cleavage of peptide linkages on the N-terminal side of Pro residues [12]. This propensity for selective fragmentation has also been reported for

singly-protonated peptides [13-18] and multiply-charged protein ions [19]. This phenomenon is sometimes known as the proline effect and was first attributed to the relatively high proton affinity of Pro [20]. Vaisar and Urban investigated a number of peptides that contained a modified amino acid residue of relatively high proton affinity, most notably one that contained a six-membered piperidine ring as opposed to Pro's five-membered pyrolidine ring, and concluded that proton affinity does not explain the proline effect [21]. They attributed the preferred N-terminal (as opposed to C-terminal) cleavage to Pro in terms of increased ring strain in forming a bicyclic b ion when the C-terminal peptide bond is cleaved. The conformation of the Pro residue may also play an important role in fragmentation. Wysocki and co-workers studied this with a database of low-energy CID tandem mass spectra of doubly-charged peptides [22]. They found that the residue (Xxx) adjacent to Pro affects the extent of fragmentation at the Xxx-Pro bond. Particularly enhanced Xxx-Pro bond cleavage when Xxx is Val, Ile, and Leu was ascribed to the steric hindrance of their bulky side chains, since it causes Pro to take a 'reactive' trans form that leads to product ions. However, they did not elucidate the 'reactive' conformation of Pro or the fragmentation mechanism. Infrared multiphoton dissociation (IRMPD) of peptides results in few backbone (*b*- and *y*-type) cleavages but increased side-chain fragmentation. In addition, IRMPD showed an increased selectivity toward N-terminal backbone cleavages to Pro [23].

In addition and complementary to CID, reactions of polypeptide ions with electrons and small radical ions, such as electron capture dissociation (ECD) [24, 25] and electron-transfer dissociation (ETD) [26-28], have become very useful tools for peptide structural analysis. The ion–electron and ion–ion reactions are different from slow heating methods, such as CID, by the fact that the intermediate fragmenting species are odd-electron ions. In fact, the presence of a radical site diminishes the strength of nearby bonds. In particular, for peptide polyanions,

preferential backbone cleavage of C–C bonds yielding a and x ions as well as side chain fragmentation were demonstrated [29-33]. Specific cleavage of peptide linkages on the N-terminal of Pro residues was also observed in ECD [31, 34, 35].

Vacuum ultraviolet photodissociation (VUVPD) is an elegant, high-energy method for inducing fragmentation in peptides [36]. Following electronic transition, direct dissociation in the excited state competes with radiative relaxation and internal conversion to the electronic ground state. VUVPD of Pro-containing peptide ions was reported with the production of unusual product ions [37]. In particular, unusual b_n+2 and a_n+2 ions were observed. Their formation was explained by homolytic cleavage of the C_α-C bond in conjunction with a rearrangement between electrons and an amide hydrogen. Formation of these abnormal ions has been compared to the effect of Pro on gas-phase conformation of peptides. UVPD of peptides at 193 nm was achieved with production of *a*, *b*, *c*, *x*, *y*, and *z* sequence ions, in addition to immonium ions and *v* and *w* side-chain loss ions [38]. However, the unusual fragment ions were not reported for the studied sequences.

Herein, we investigate the UVPD of Pro-containing peptides at 213 nm. This wavelength corresponds to the emergence of the lowest-lying electronic excited states of the molecules and thus allows the investigation of the relation between the nature of excited states and the observed fragmentation patterns. The calculation of the electronic excited states and molecular dynamics for the model RPK peptide (arginine-proline-lysine) are reported here in order to gain insight into the first steps of UV photodissociation of Pro-containing peptides. Our complementary theoretical and experimental investigations open a new route for identification of the photofragmentation pathways allowing identification of the link between the nature of electronic excited states and the observed fragmentation pathways.

Material and methods

Chemicals

Methanol (MeOH) was obtained from Fisher Scientific (Strasbourg, France) and milli-Q water (18.2 MΩ.cm) was used. Deuterated methanol (CH_3OD), deuterium oxide (D_2O), Bradykinin and Substance P acetate salts were purchased from Sigma–Aldrich (St Quentin-Fallavier, France). LGPLVEQGR, LGADMEDVR and EANYIGSDK peptides were synthesized by Millegen (Labège, France). RPK peptide was synthesized by GeneCust (Dudelange, Luxembourg).

Instrumentation

Experiments were performed on a hybrid quadrupole-orbitrap Q-Exactive® mass spectrometer (Thermo Fisher Scientific, San Jose, CA, USA) equipped with a HESI ion source. The instrument was modified to allow UV laser irradiation of ions. A schematic of the photo-dissociation set-up is given in Figure 1. A quartz window was fitted on the rear of the HCD (High Collision Dissociation) cell to permit introduction of a laser beam. The detector plate, initially positioned at the exit of the HCD cell and on the laser beam trajectory, was removed. The laser is a BrillantBNd:YAG (from Quantel, Les Ulis, France). The 5th harmonic at λ=213 nm was used with a repetition rate of 20 Hz. This harmonic is generated by combination of the fundamental and 4th harmonic. For experiments at 266 nm, the 4th harmonic was used. The laser beam passes through lenses, diaphragms and is injected in the HCD cell using two dichroic mirrors. The laser beam energy irradiating the ions was ~ 1 mJ/pulse. The laser is slightly off axis in order to avoid photo-fragmentation in the C-trap.

Mass Spectrometry Operating Conditions

Ionization was achieved using an electrospray in positive ionization mode with an ion spray voltage of 4 500 V. The sheath gas and auxiliary gas (nitrogen) flow rates were set at 20 and 15 (arbitrary unit), respectively, with a HESI vaporizer temperature of 250 °C. The ion transfer capillary temperature was 250 °C. The S-lens RF was set at 90 (arbitrary unit). The orbitrap resolution was 140 000. The Automatic Gain Control (AGC) target was 3e6 and the maximum injection time was set at 250 ms. For LID (laser-induced dissociation) experiments, the HCD parameters were optimized in order to avoid CID and were set at 2 eV for the collision energy and 1000 ms for the activation time. CID experiments were performed using a normalized collision energy of 25 % and 3 ms activation time. An *m/z* window of 2.0 Th was applied for precursor isolation. Peptides were dissolved in 50/50 MeOH/water (vol/vol) at a concentration of 100 µM and directly electrosprayed at a flow rate of 5 µL/min.

Computation

Investigation of the structures of the RPK model system (arginine+proline+lysine) was done using the simulated annealing method coupled to molecular dynamic simulations using the semi-empirical AM1 method [39]. The structures found were then re-optimized using the semi-empirical OM2 (orthogonalization model 2) method [40]. To calculate the absorption spectra, the OM2 method combined with the graphical unitary group approach (GUGA) multi-reference configuration interaction (MR-CI) [41, 42] within the MNDO program [43] was used. The active space which consists of five occupied and five virtual orbitals was chosen, and all single, double, and triple excitations out of the self-consistent field reference configurations were included in the calculations.

Since the experiments were done at a temperature close to 300 K, we simulated the thermally-broadened absorption spectra. The configurations were sampled from a long molecular dynamic trajectory run at a constant temperature of 300 K using the semi-empirical OM2 method. To simulate the temperature broadening of the spectrum, the absorption spectrum for each configuration was calculated and these spectra were superimposed. The non-adiabatic dynamics "on the fly" in electronic excited states were determined using Tully's surface-hopping algorithm with non-adiabatic couplings [44]. The initial conditions for non-adiabatic dynamics were obtained by sampling 100 coordinates and momenta along a 30 ps ground-state trajectory at a constant temperature of 300 K using the OM2 method. The nuclear trajectories were propagated by numerical solution of Newton's equations of motion using the Verlet velocity algorithm [45] with a time step of 0.1 fs. The non-adiabatic dynamics were determined starting from S_2 or S_3 state matching experimental conditions.

Results and discussion

The LID of Pro-containing peptides

The 213 nm LID of the doubly-protonated $[M+2H]^{2+}$ (*m/z* 530.79) of Bradykinin (RPPGFSPFR) is shown in Figure 2a. A series of singly-charged $(y_n)^+$, $(b_n)^+$ and $(a_n)^+$ ions are mainly observed with a 10% relative intensity. $(y_n)^+$ ions are detected for n = 2 to 4 and 6 to 8. $(b_n)^+$ ions are detected for n = 1, 2 and 6 to 8, while $(a_n)^+$ ions are detected for n = 1, 2, 5, 6 and 8. The $(z_3)^+$ ion is also detected at *m/z* 402.21 as well as doubly-charged $(y_8)^{2+}$ at *m/z* 452.74. The peptide sequence can be confirmed with these backbone fragment ions. The immonium ion of the phenylalanine residue $[F]^+$ is detected at *m/z* 120.08. Loss of a water molecule from the doubly-charged ion precursor is also observed yielding the $[M+2H-H_2O]^{2+}$

ion (*m/z* 521.78). Charge reduced $[M+H]^+$ is detected at *m/z* 1060.57. We assigned these fragment ions and confirmed them by the exact masses reported in Table 1. The errors were all less than 2 ppm. For comparison, the CID spectrum of doubly-protonated $[M+2H]^{2+}$ (*m/z* 530.79) of Bradykinin is shown in Figure 2b. Backbone fragment ions are also observed as well as water elimination and the $[M+H]^+$ ion (Table 1).

More interestingly, LID at 213 nm generates new fragments that are not observed in the CID spectrum. The assignment of these ions was confirmed by the exact masses (Table 1). Fragment ions detected at *m/z* 902.46, *m/z* 805.40 and *m/z* 417.22 correspond to the elemental composition of y ions minus 2 hydrogens and have been labeled in Figure 2a $(y_8\text{-}2)^+$, $(y_7\text{-}2)^+$ and $(y_3\text{-}2)^+$, respectively. These y_n-2 ions are not observed along the whole peptide sequence. This fragmentation pathway occurs only with a Pro residue. In fact, Bradykinin contains 3 Pro residues Pro2, Pro3 and Pro7 among a total of 9 amino acid residues giving rise to $(y_8\text{-}2)^+$, $(y_7\text{-}2)^+$ and $(y_3\text{-}2)^+$ ions. These ions are more intense compared to their homologue y_n ions. The relative intensities of $(y_8\text{-}2)^+$, $(y_7\text{-}2)^+$ and $(y_3\text{-}2)^+$ ions correspond to 50 %, 150 % and 300 % of the relative intensities of $(y_8)^+$, $(y_7)^+$ and $(y_3)^+$, respectively. Fragment ions detected at *m/z* 159.12, *m/z* 256.18 and *m/z* 644.35 have the elemental composition of b ions plus 2 hydrogens and, in Figure 2a, have been labeled $(b_1\text{+}2)^+$, $(b_2\text{+}2)^+$ and $(b_6\text{+}2)^+$, respectively. This fragmentation reaction is very efficient compared to the classical mechanism as the relative intensities of $(b_1\text{+}2)^+$, $(b_2\text{+}2)^+$ and $(b_6\text{+}2)^+$ ions represent 400, 500 and 700 % of the relative intensities of their b_n homologues. The same behavior is observed for the fragment ions detected at *m/z* 131.13, *m/z* 228.18 and *m/z* 616.36 which correspond to a_n ions plus 2 hydrogens and, in Figure 2a, have been labeled $(a_1\text{+}2)^+$, $(a_2\text{+}2)^+$ and $(a_6\text{+}2)^+$, respectively. Furthermore, these ions are only observed in the neighborhood of the Pro residues. The $(x_3)^+$

ion is detected at *m/z* 348.17 in the LID spectrum. Kim *et al.* [37] also observed these unusual fragment ions in the LID of singly-charged Pro-containing peptides at 157 nm.

The same LID experiment was done for the doubly-protonated $[M+2H]^{2+}$ of Substance P (RPKPQQFFGLM) (*m/z* 674.86) and LGPLVEQGR (*m/z* 484.77) peptides. The spectra are shown in Figures S1 and S2 in the Supporting material. Besides the backbone fragments y_n, b_n and a_n observed in LID and CID, LID spectra show y_n-2, b_n+2 and a_n+2 fragment ions. For the doubly-protonated Substance P peptide which contains 2 Pro residues Pro2 and Pro4, $(y_{10}-2)^+$ and $(y_8-2)^+$ ions are detected at *m/z* 1190.60 and *m/z* 965.45 corresponding to y ions minus 2 hydrogens (according to exact masses). b and a fragment ions plus 2 hydrogens $(a_1+2)^+$, $(b_1+2)^+$, $(a_3+2)^+$ and $(b_3+2)^+$ are detected at *m/z* 131.12, *m/z* 159.12, *m/z* 356.19 and *m/z* 384.26, respectively. The $(x_7)^+$ ion is detected at *m/z* 640.28 in the LID spectrum. All assignment errors were less than 1.3 ppm. In the LID spectrum of doubly-protonated LGPLVEQGR, which has a Pro3 residue among a total of 9 amino acid (AA) residues, $(y_7-2)^+$, $(a_2+2)^+$ and $(b_2+2)^+$ are detected at *m/z* 796.43, *m/z* 173.13 and *m/z* 145.13, respectively (Figure S2). From these 3 examples, we can conclude that $(y_n-2)^+$ ions are only observed in LID for n = (total number of AA - #Pro + 1). These ions still contain the Pro residue. On the other hand, $(b_n+2)^+$ and $(a_n+2)^+$ ions are only observed in LID for n = (#Pro - 1), and they do not contain the Pro residue. These fragmentation pathways are observed only with cleavage of bonds between the amino acid N-terminal to Pro and the Pro residue. In order to confirm the contribution of the Pro residue in these fragmentation pathways, LID experiments were done at 213 nm for doubly-protonated ions of LGADMEDVR (*m/z* 503.24) and EANYIGSDK (*m/z* 498.74) peptides that do not contain Pro. The LID spectra are presented in Figures S3 and S4, respectively. In these cases, CID and LID spectra are similar. No $(y_n-2)^+$, $(b_n+2)^+$ or $(a_n+2)^+$ ions are detected in LID. Therefore, the effect of the excited Pro residue is clearly evident in

these new mechanisms. Note that LID experiments were also done at 266 nm for the Pro-containing peptides and new fragment ions were not observed (data not shown). The fact that no unusual fragments close to the Pro were observed means that a higher energy UV excitation (below 266 nm) is required to induce these specific photo-fragments.

LID and optical properties of the protonated RPK model peptide

In order to understand the proline effect, the specificity of VUV excitation and the mechanisms involved in the formation of the unusual fragment ions, a model RPK peptide was used for LID experiments at 213 nm. The optical properties were calculated in parallel to the experiments. Figure 3a shows the 213 nm LID mass spectrum of the singly-protonated $[M+H]^+$ (*m/z* 400.27) of RPK peptide. Singly-charged $(y_1\text{-}2)^+$, $(b_1\text{-}2)^+$ and $(a_1\text{-}2)^+$ ions are mainly observed with a 20% relative intensity. The immonium ion of the Pro residue $[P]^+$ is detected at *m/z* 70.07. We observed that one and two water molecules were lost from the precursor ion yielding the $[M+H\text{-}H_2O]^+$ ion (*m/z* 382.26) and $[M+H\text{-}2H_2O]^+$ ion (*m/z* 364.25). The fragment ion detected at *m/z* 341.22 arises from the loss of C_3H_7O from the precursor ion. The errors were all less than 1.7 ppm. The CID spectrum of the protonated $[M+H]^+$ (*m/z* 400.27) of RPK is used as a reference in Figure 3b. Intense backbone fragment ions are also observed as well as water eliminations and $[P]^+$ (Table 2). The LID of the protonated RPK peptide ion also shows the unusual $(y_2\text{-}2)^+$, $(x_1)^+$, $(b_1+2)^+$ and $(a_1+2)^+$ ions detected at *m/z* 242.15, *m/z* 173.06, *m/z* 159.12 and *m/z* 131.13, respectively (Figure 3a), in contrast to the CID spectrum. All the assignments were confirmed by exact masses (Table 2).

The structural properties of $[M+H]^+$ of the RPK model system were determined via semi-empirical calculations (OM2) as described in the computational section. A number of structures with different binding sites for protons were explored and the lowest energy one has a proton bound to the Arginine side chain NH group (pKa value=12). The calculated OM2

spectrum at T=0 K for the lowest energy structure is shown in Figure 4a. The absorption features are characterized by a dominant transition to the S_5 excited state at 195 nm. Transition to S_2 and S_3 excited states with weaker intensity at 214 nm and 207 nm are close to the wavelength used for LID experiments (213 nm). Figure 4a also shows analysis of excitations for the three lowest transitions of the protonated RPK model system in the gas phase. Although, single, double and triple electron excitations were included in calculations, only single excitations have significant contributions in the transitions. Excitations around 200 nm correspond to those of the Pro residue and from the C- and N-terminus of the RPK model system. The lowest excited state S_1 at 236 nm is characterized by a transition from the p orbital of the C atom to the p orbital of the N atom in the Arginine backbone, while the excitation from the p orbital of the N atom to the p orbital of the C atom of the Lysine backbone is characteristic of the transition to the S_2 excited state. The most intense transition to S_5 is dominated by excitation from the p orbital on the N atom in the Lysine backbone to the p orbital on the C atom in Pro.

Since the experiment is performed at a temperature close to 300 K, we calculated the thermally-broadened spectrum at 300 K, shown in Figure 4b, and found that the highest density of transitions occurred around 213 nm due to S_2 and S_3 excited states. Therefore, in order to follow fragmentation pathways, the non-adiabatic dynamics were studied starting from the S_2 and S_3 states. However, as they both proceed through similar pathways, the equivalent fragmentation pathways were observed. Therefore, we present results obtained starting from the S_2 state only.

Non-adiabatic molecular dynamics for the fragmentation of protonated RPK peptide

The non-adiabatic dynamics at 300 K starting from the second excited state S_2 lead to major fragmentation pathways which take place in the S_1 state, after non-adiabatic transitions from

higher excited states, as illustrated in Figure 5. The pathways include C-N bond (Arg-Pro) breaking, and breaking of C-C bonds in the Arginine and Pro backbones. Snapshots at different times along selected trajectories illustrating bond breaking are shown in Figure 5. The dominant excitations among molecular orbitals in the S_1 state at the time of bond breaking are also presented, illustrating the nature of the fragmentation pathways. C-N bond breaking (Figure 5a, at 82 fs) is characterized by excitation from the nonbonding HOMO to the antibonding LUMO localized at N and C atoms. The breaking of the C-C bond in Pro occurs at 18 fs (Figure 5b) and is characterized by excitations from the nonbonding HOMO to the LUMO localized at the C_α atom and C atom from the carbonyl group of Pro, respectively. The trajectory showing C-C bond breaking in Arginine which is followed by proton transfer is presented in Figure 5c. After proton transfer, the Arginine fragment is unstable, and rearrangement of protons can be expected. At 30 fs, the C-C bond in Arginine breaks (see Figure 5c) and so the S_1 state for this structure is characterized by excitations from orbitals localized on the Arginine and Pro backbone to the antibonding (C-C in Arginine backbone) molecular orbital (see the bottom of Figure 5c). At ~75 fs, proton transfer as well as return to the ground state occur. The above analysis explains that different fragmentation pathways involving specific bond breaking in the S_1 state occur due to non-adiabatic transitions between different electronic excited states. To summarize, the excitations to S_2 and S_3 states result in fast non-adiabatic transitions to the S_1 state followed by activation of C-C and C-N bonds close to the Pro residues.

Fragmentation mechanisms of the protonated RPK peptide

Interestingly, the above activations are the first steps in the formation of the fragment ions observed experimentally (i.e. (y-2), (a+2) and (b+2)). Trajectories shown in Figure 5a correspond to the homolytic cleavage of the C-N peptide bond close to Pro which is the first

step in generating (y-2) type fragments. In fact, simultaneous rearrangement and elimination of CO and two H radicals, from the N-terminus and CH_2 group of the Pro ring, would yield the $(y_2\text{-}2)^+$ fragment ion at *m/z* 242.15 when the charge is on the lysine side chain at the time of the dissociation, as proposed in Scheme 1a. The complementary $(a_1)^+$ ion at *m/z* 129.11 would be produced via the same mechanism if the charge was located on the arginine (Arg) residue (Scheme 1a).

The $(b_2+2)^+$ fragment ion, detected at *m/z* 159.12, would be formed when the Arg side chain bears the charge. The mechanism involves first C-C bond activation then breaking in the Pro residue (shown in Figure 5b) and finally, proton transfer from the amine of the lysine (Lys) residue to the carbonyl group of the Arg, according to Scheme 1b. The $(x_1)^+$ ion at *m/z* 173.06 is generated with the same mechanism if the charge is located on the Lys residue rather than the N-terminus.

In the same way, trajectories reported in Figure 5c lead to the C_α-C bond breaking on the N-terminal side of Pro which is a prerequisite for generating (a+2) type fragments. Additional proton transfer from the CH_2 of the Pro ring to the alkyl group of the Arg and elimination of a CO molecule (presented in Scheme 1c) would produce the $(a_1+2)^+$ ion detected at *m/z* 131.13 when the Arg side chain bears the charge. This fragmentation pathway would also lead to the $(y_2\text{-}2)^+$ fragment ion if the charge is located on the Lys residue at the time of the dissociation.

Since the above mechanisms involve exchangeable hydrogen atoms, they could be tested by performing H/D exchange experiments. The LID-MS/MS spectrum of the singly-charged RPK peptide detected at *m/z* 411.34 after ESI of the CH_3OD/D_2O 50:50 (% v/v) solution of the RPK peptide is shown in Figure 6. In this case, all 11 mobile hydrogens have been exchanged, as highlighted in red in Scheme 2. The single charge is located either on $=NH_2^+$ of the Arg or on the NH_3^+ of the Lys residue (Scheme 2). The singly-charged d_{11}-RPK precursor

ion was then detected with an 11 Da mass increase. Similarly, a, b and y ions as well as deuterium oxide losses (see assignments in Table 3) are observed in the LID from this precursor. The LID at 213 nm of the singly-charged d_{11}-RPK also shows (Figure 6) the unusual d_5-$(y_2\text{-}2)^+$, d_4-$(x_1)^+$, d_8-$(b_1+2)^+$ and d_7-$(a_1+2)^+$ ions detected at *m/z* 247.18, *m/z* 177.12, *m/z* 167.17 and *m/z* 138.17, respectively (exact masses in Table 3). Comparison of fragmentation patterns in Figures 3a and 6 confirms the proposed mechanism. First, fragment $(y_2\text{-}2)^+$ presents a 5 Da mass increase in agreement with structures proposed in Scheme 1a and 1c i.e. one deuterium on the Lys amine, three deuterium on the Lys side chain bearing the charge, and one deuterium on the C-terminus group. Moreover, the $(a_1)^+$ fragment is detected with a 6 Da mass increase (Figure 6) after H/D exchange as expected from the structure in Scheme 1a i.e. five deuterium on the Arg side chain bearing the charge and one on the N-terminus. In fact, the precursor ion has eliminated a deuterium from the initial ND_2 terminus group which confirms the mechanism in Scheme 1a. In addition, according to the mechanism proposed in Scheme 1b, $(x_1)^+$ should have three deuterium on the Lys side chain bearing the charge and one at the C-terminus group, i.e. a 4 Da mass increase. This is observed (Figure 6). Again following Scheme 1b, fragment $(b_1+2)^+$ should contain five deuterium on the Arg side chain bearing the charge, two at the N-terminus group and one on the Arg carbonyl group where it has been transferred from the Lys amine group, i.e. an 8 Da mass increase, which is also observed on the fragmentation pattern (Figure 6). Therefore, up to this point, all examined fragmentation pathways are in agreement with the mechanisms previously proposed by Kim *et al.* [37].

Finally, the $(a_1+2)^+$ fragment is detected with a 7 Da mass increase (Figure 6) which is inconsistent with a proton transfer from the Lys amine as proposed by Kim *et al.* [37] which would have led to an 8 Da mass increase. Alternatively, a proton transfer from a CH_2 group of

the Pro ring, as proposed in Scheme 1c, would explain the observed 7 Da mass increase, i.e. five deuterium on the Arg side chain bearing the charge and two deuterium at the N-terminal. Moreover, we can note that the relative intensity between the $(a_1\text{-}2)^+$ and $(a_1)^+$ ions is the same (73%) before and after H/D exchange (Figures 3a and 6). This confirms the proposed mechanism where D transfer is not required. In fact, hydrogen migration is favored over deuterium transfer.

Conclusions

To conclude, we observed the formation of unusual (y-2), (a+2) and (b+2) fragment ions upon laser-induced dissociation of proline-containing peptides at 213 nm. The formation of these ions was not observed at 266 nm, or for non-proline-containing peptides. The RPK peptide was the smallest peptide for which we were able to observe these fragmentation pathways experimentally. Calculation of the electronic excited states for this peptide showed that S_2 and S_3 states could be excited at the experimental wavelength. Non-adiabatic molecular dynamic simulation (MD) starting from S_2 and S_3 excited states showed that this excitation was followed by C-C and C-N bond activation close to the proline residue. The MD revealed early relaxation mechanisms leading to the observed fragmentation pathways.

Our complementary theoretical and experimental investigations open new routes for identification of photofragmentation pathways. They enable the identification of the link between the nature of electronically-excited states and the observed fragmentation pathways. The MD simulations on the fly provide the foundation for a molecular understanding of the photochemistry of peptides under UV excitation. These trajectories revealed specific breaking of C-C and C-N bonds close to the proline residue. Consecutive rearrangements and proton

transfers are required to produce the above unusual fragment ions and the fragmentation mechanisms were confirmed by H/D exchange experiments.

Acknowledgment

V.B.-K. and P. D. would like to thank the CNRS NCBA international laboratory. V.B.-K. gratefully acknowledges support from the Deutsche Forschungsgemeinschaft (DFG FOR1282) and Split-Dalmatia County. The research leading to these results has received funding from the European Research Council under the European Union's Seventh Framework Programme (FP7/2007-2013 Grant agreement N°320659).

References

1. Paizs, B.; Suhai, S.: Fragmentation pathways of protonated peptides. Mass Spectrom. Rev. **24**(4), 508-548 (2005)
2. Smith, R. D.; Loo, J. A.; Loo, R. R. O.; Busman, M.; Udseth, H. R.: Principles and Practice of Electrospray Ionization - Mass-Spectrometry for Large Polypeptides and Proteins. Mass Spectrom. Rev. **10**(5), 359-451 (1991)
3. Cox, K. A.; Gaskell, S. J.; Morris, M.; Whiting, A.: Role of the site of protonation in the low-energy decompositions of gas-phase peptide ions. J. Am. Soc. Mass. Spectrom. **7**(6), 522-531 (1996)
4. Dongre, A. R.; Jones, J. L.; Somogyi, A.; Wysocki, V. H.: Influence of peptide composition, gas-phase basicity, and chemical modification on fragmentation efficiency: Evidence for the mobile proton model. J. Am. Chem. Soc. **118**(35), 8365-8374 (1996)
5. Dongre, A. R.; Somogyi, A.; Wysocki, V. H.: Surface-induced dissociation: An effective tool to probe structure, energetics and fragmentation mechanisms of protonated peptides. J. Mass Spectrom. **31**(4), 339-350 (1996)
6. Jones, J. L.; Dongre, A. R.; Somogyi, A.; Wysocki, V. H.: Sequence Dependence of Peptide Fragmentation Efficiency Curves Determined by Electrospray-Ionization Surface-Induced Dissociation Mass-Spectrometry. J. Am. Chem. Soc. **116**(18), 8368-8369 (1994)
7. Summerfield, S. G.; Bolgar, M. S.; Gaskell, S. J.: Promotion and stabilization of b(1) ions in peptide phenylthiocarbamoyl derivatives: Analogies with condensed-phase chemistry. J. Mass Spectrom. **32**(2), 225-231 (1997)
8. Summerfield, S. G.; Whiting, A.; Gaskell, S. J.: Intra-ionic interactions in electrosprayed peptide ions. Int. J. Mass Spectrom. Ion Processes **162**(1-3), 149-161 (1997)
9. Hunt, D. F.; Yates, J. R.; Shabanowitz, J.; Winston, S.; Hauer, C. R.: Protein Sequencing by Tandem Mass-Spectrometry. Proc. Natl. Acad. Sci. U.S.A. **83**(17), 6233-6237 (1986)
10. Johnson, R. S.; Martin, S. A.; Biemann, K.: Collision-Induced Fragmentation of (M+H)+Ions of Peptides - Side-Chain Specific Sequence Ions. Int. J. Mass Spectrom. Ion Processes **86**, 137-154 (1988)
11. Tabb, D. L.; Smith, L. L.; Breci, L. A.; Wysocki, V. H.; Lin, D.; Yates, J. R.: Statistical characterization of ion trap tandem mass spectra from doubly charged tryptic peptides. Anal. Chem. **75**(5), 1155-1163 (2003)
12. Reid, G. E.; Wu, J.; Chrisman, P. A.; Wells, J. M.; McLuckey, S. A.: Charge-state-dependent sequence analysis of protonated ubiquitin ions via ion trap tandem mass spectrometry. Anal. Chem. **73**(14), 3274-3281 (2001)
13. Counterman, A. E.; Clemmer, D. E.: Cis-trans signatures of proline-containing tryptic peptides in the gas phase. Anal. Chem. **74**(9), 1946-1951 (2002)
14. Harrison, A. G.; Young, A. B.: Fragmentation reactions of deprotonated peptides containing proline. The proline effect. J. Mass Spectrom. **40**(9), 1173-1186 (2005)
15. Hayakawa, S.; Hashimoto, M.; Matsubara, H.; Turecek, F.: Dissecting the proline effect: Dissociations of proline radicals formed by electron transfer to protonated pro-gly and gly-pro dipeptides in the gas phase. J. Am. Chem. Soc. **129**(25), 7936-7949 (2007)
16. Ramek, M.; Kelterer, A. M.; Teppen, B. J.; Schafer, L.: Theoretical Structure Investigations of N-Acetyl-L-Proline Amide. J. Mol. Struct. **352**, 59-70 (1995)
17. Vaisar, T.; Urban, J.: Probing the proline effect in CID of protonated peptides. Journal of Mass Spectrometry **31**(10), 1185-1187 (1996)

18. Vanhoof, G.; Goossens, F.; Demeester, I.; Hendriks, D.; Scharpe, S.: Proline Motifs in Peptides and Their Biological Processing. FASEB J. **9**(9), 736-744 (1995)
19. Loo, J. A.; Edmonds, C. G.; Smith, R. D.: Tandem Mass-Spectrometry of Very Large Molecules .2. Dissociation of Multiply Charged Proline-Containing Proteins from Electrospray Ionization. Anal. Chem. **65**(4), 425-438 (1993)
20. Schwartz, B. L.; Bursey, M. M.: Some Proline Substituent Effects in the Tandem Mass-Spectrum of Protonated Pentaalanine. Biol. Mass Spectrom. **21**(2), 92-96 (1992)
21. Vaisar, T.; Urban, J.: Probing the proline effect in CID of protonated peptides. J. Mass Spectrom. **31**(10), 1185-1187 (1996)
22. Breci, L. A.; Tabb, D. L.; Yates, J. R.; Wysocki, V. H.: Cleavage N-terminal to proline: Analysis of a database of peptide tandem mass spectra. Anal. Chem. **75**(9), 1963-1971 (2003)
23. Madsen, J. A.; Gardner, M. W.; Smith, S. I.; Ledvina, A. R.; Coon, J. J.; Schwartz, J. C.; Stafford, G. C., Jr.; Brodbelt, J. S.: Top-Down Protein Fragmentation by Infrared Multiphoton Dissociation in a Dual Pressure Linear Ion Trap. Analytical Chemistry **81**(21), 8677-8686 (2009)
24. Zubarev, R. A.: Reactions of polypeptide ions with electrons in the gas phase. Mass Spectrometry Reviews **22**(1), 57-77 (2003)
25. Zubarev, R. A.; Kelleher, N. L.; McLafferty, F. W.: Electron capture dissociation of multiply charged protein cations. A nonergodic process. J. Am. Chem. Soc. **120**(13), 3265-3266 (1998)
26. Coon, J. J.; Shabanowitz, J.; Hunt, D. F.; Syka, J. E. P.: Electron transfer dissociation of peptide anions. J. Am. Soc. Mass. Spectrom. **16**(6), 880-882 (2005)
27. Mikesh, L. M.; Ueberheide, B.; Chi, A.; Coon, J. J.; Syka, J. E. P.; Shabanowitz, J.; Hunt, D. F.: The utility of ETD mass spectrometry in proteomic analysis. Biochim. Biophys. Acta **1764**(12), 1811-1822 (2006)
28. Syka, J. E. P.; Coon, J. J.; Schroeder, M. J.; Shabanowitz, J.; Hunt, D. F.: Peptide and protein sequence analysis by electron transfer dissociation mass spectrometry. Proc. Natl. Acad. Sci. U.S.A. **101**(26), 9528-9533 (2004)
29. Antoine, R.; Joly, L.; Tabarin, T.; Broyer, M.; Dugourd, P.; Lemoine, J.: Photo-induced formation of radical anion peptides. Electron photodetachment dissociation experiments. Rapid Commun. Mass Spectrom. **21**(2), 265-268 (2007)
30. Anusiewicz, I.; Jasionowski, M.; Skurski, P.; Simons, J.: Backbone and side-chain cleavages in electron detachment dissociation (EDD). J. Phys. Chem. A **109**(49), 11332-11337 (2005)
31. Kjeldsen, F.; Silivra, O. A.; Ivonin, I. A.; Haselmann, K. F.; Gorshkov, M.; Zubarev, R. A.: C-alpha-C backbone fragmentation dominates in electron detachment dissociation of gas-phase polypeptide polyanions. Chem. Eur. J. **11**(6), 1803-1812 (2005)
32. Larraillet, V.; Antoine, R.; Dugourd, P.; Lemoine, J.: Activated-Electron Photodetachment Dissociation for the Structural Characterization of Protein Polyanions. Anal. Chem. **81**(20), 8410-8416 (2009)
33. Larraillet, V.; Vorobyev, A.; Brunet, C.; Lemoine, J.; Tsybin, Y. O.; Antoine, R.; Dugourd, P.: Comparative Dissociation of Peptide Polyanions by Electron Impact and Photo-Induced Electron Detachment. J. Am. Soc. Mass. Spectrom. **21**(4), 670-680 (2010)
34. Cook, S. L.; Collin, O. L.; Jackson, G. P.: Metastable atom-activated dissociation mass spectrometry: leucine/isoleucine differentiation and ring cleavage of proline residues. J. Mass Spectrom. **44**(8), 1211-1223 (2009)

35. Cooper, H. J.; Hudgins, R. R.; Hakansson, K.; Marshall, A. G.: Secondary fragmentation of linear peptides in electron capture dissociation. Int. J. Mass Spectrom. **228**(2-3), 723-728 (2003)
36. Reilly, J. P.: Ultraviolet Photofragmentation of Biomolecular Ions. Mass Spectrom. Rev. **28**(3), 425-447 (2009)
37. Kim, T.-Y.; Valentine, S. J.; Clemmer, D. E.; Reilly, J. P.: Gas-Phase Conformation-Specific Photofragmentation of Proline-Containing Peptide Ions. J. Am. Soc. Mass. Spectrom. **21**(8), 1455-1465 (2010)
38. Madsen, J. A.; Boutz, D. R.; Brodbelt, J. S.: Ultrafast Ultraviolet Photodissociation at 193 nm and its Applicability to Proteomic Workflows. J. Proteome Res. **9**(8), 4205-4214 (2010)
39. Dewar, M. J. S.; Zoebisch, E. G.; Healy, E. F.; Stewart, J. J. P.: The Development and Use of Quantum-Mechanical Molecular-Models .76. Am1 - a New General-Purpose Quantum-Mechanical Molecular-Model. J. Am. Chem. Soc. **107**(13), 3902-3909 (1985)
40. Weber, W.; Thiel, W.: Orthogonalization corrections for semiempirical methods. Theor. Chem. Acc. **103**(6), 495-506 (2000)
41. Patchkovskii, S.; Koslowski, A.; Thiel, W.: Generic implementation of semi-analytical CI gradients for NDDO-type methods. Theor. Chem. Acc. **114**(1-3), 84-89 (2005)
42. Koslowski, A.; Beck, M. E.; Thiel, W.: Implementation of a general multireference configuration interaction procedure with analytic gradients in a semiempirical context using the graphical unitary group approach. J. Comput. Chem. **24**(6), 714-726 (2003)
43. Thiel, W. *MNDO program.*, Max-Planck-Institut für Kohlenforschung: Muhlheim, Germany: 2007.
44. Tully, J. C.: Molecular-Dynamics with Electronic-Transitions. J. Chem. Phys. **93**(2), 1061-1071 (1990)
45. Verlet, L.: Computer Experiments on Classical Fluids .I. Thermodynamical Properties of Lennard-Jones Molecules. Phys. Rev. **159**(1), 98-& (1967)

Table 1. Exact masses and assignments of fragment ions detected in the LID and CID spectra of doubly-protonated Bradykinin $[M+2H]^{2+}$ (Figure 2). Error = (*m/z* theoretical – *m/z* experimental)/(*m/z* theoretical)

Assignment	Elemental composition	Theoretical *m/z*	LID		CID	
			Experimental *m/z*	Error (ppm)	Experimental *m/z*	Error (ppm)
$[M+H]^+$	$C_{50}H_{74}O_{11}N_{15}$	1060.5687	1060.5693	0.566	1060.5694	0.660
$[M+H-C_3H_7O]^+$	$C_{47}H_{67}O_{10}N_{15}$	1001.5190	ND	NA	1001.5197	0.699
$(y_8)^+$	$C_{44}H_{62}O_{10}N_{11}$	904.4676	904.4673	-0.332	904.4680	0.442
$(y_8\text{-}2)^+$	$C_{44}H_{60}O_{10}N_{11}$	902.4550	902.4553	0.377	ND	NA
$(b_8)^+$	$C_{44}H_{60}O_9N_{11}$	886.4570	886.4573	0.338	886.4575	0.564
$(a_8)^+$	$C_{43}H_{60}O_8N_{11}$	858.4621	858.4628	0.815	858.4625	0.466
$(y_7)^+$	$C_{39}H_{55}O_9N_{10}$	807.4148	807.4153	0.619	807.4152	0.495
$(y_7\text{-}2)^+$	$C_{39}H_{53}O_9N_{10}$	805.3991	805.3995	0.497	ND	NA
$(z_7)^+$	$C_{39}H_{52}O_9N_9$	790.3883	ND	NA	790.3880	-0.380
$(b_7)^+$	$C_{35}H_{51}O_8N_{10}$	739.3886	739.3892	0.811	739.3889	0.406
$(y_6)^+$	$C_{34}H_{48}O_8N_9$	710.3620	710.3616	-0.563	710.3624	0.563
$(y_5)^+$	$C_{32}H_{45}O_7N_8$	653.3406	ND	NA	653.3409	0.459
$(b_6+2)^+$	$C_{30}H_{46}O_7N_9$	644.3515	644.3518	0.466	ND	NA
$(b_6)^+$	$C_{30}H_{44}O_7N_9$	642.3358	642.3360	0.311	642.3361	0.467
$(a_6+2)^+$	$C_{29}H_{46}O_6N_9$	616.3566	616.3563	-0.487	ND	NA
$(a_6)^+$	$C_{29}H_{44}O_6N_9$	614.3409	614.3406	-0.488	614.3412	0.488
$(b_5)^+$	$C_{27}H_{39}O_5N_8$	555.3038	ND	NA	555.3040	0.342
$[M+2H]^{2+}$	$C_{50}H_{75}O_{11}N_{15}$	530.7880	530.7877	-0.565	530.7883	0.565
$(a_5)^+$	$C_{26}H_{39}O_4N_8$	527.3089	527.3093	0.759	527.3092	0.569
$[M+2H-H_2O]^{2+}$	$C_{50}H_{73}O_{10}N_{15}$	521.7827	521.7824	-0.575	521.7831	0.767

$(y_4)^+$	$C_{23}H_{36}O_6N_7$	506.2722	506.2718	-0.790	506.2724	0.395
$(y_8)^{2+}$	$C_{44}H_{63}O_{10}N_{11}$	452.7374	452.7371	-0.663	452.7371	-0.663
$(y_3)^+$	$C_{20}H_{31}O_4N_6$	419.2401	419.2399	-0.477	419.2397	-0.954
$(y_3\text{-}2)^+$	$C_{20}H_{29}O_4N_6$	417.2245	417.2242	-0.719	ND	NA
$(b_4)^+$	$C_{18}H_{30}O_4N_7$	408.2354	ND	NA	408.2350	-0.980
$(y_7)^{2+}$	$C_{39}H_{56}O_9N_{10}$	404.2110	ND	NA	404.2108	-0.495
$(z_3)^+$	$C_{20}H_{28}O_4N_5$	402.2136	402.2131	-1.243	402.2134	-0.497
$(x_2)^+$	$C_{16}H_{22}O_4N_5$	348.1666	348.1668	0.574	ND	NA
$(y_2)^+$	$C_{15}H_{24}O_3N_5$	322.1874	322.1873	-0.310	322.1870	-1.242
$(b_2\text{+}2)^+$	$C_{11}H_{22}O_2N_5$	256.1768	256.1767	-0.390	ND	NA
$(b_2)^+$	$C_{11}H_{20}O_2N_5$	254.1612	254.1609	-1.180	254.1610	-0.787
$(a_2\text{+}2)^+$	$C_{10}H_{22}ON_5$	228.1819	228.1820	0.438	ND	NA
$(a_2)^+$	$C_{10}H_{20}ON_5$	226.1662	226.1663	0.442	226.1664	0.884
$(y_1)^+$	$C_6H_{15}O_2N_4$	175.1190	ND	NA	175.1191	0.571
$(b_1\text{+}2)^+$	$C_6H_{15}ON_4$	159.1240	159.1239	-0.628	ND	NA
$(b_1)^+$	$C_6H_{13}ON_4$	157.1084	157.1082	-1.273	157.1081	-1.910
$(a_1\text{+}2)^+$	$C_5H_{15}N_4$	131.1291	131.1290	-0.991	ND	NA
$(a_1)^+$	$C_5H_{13}N_4$	129.1135	129.1133	-1.549	129.1133	-1.549
$[F]^+$	$C_8H_{10}N$	120.0808	120.0809	1.166	120.0807	-1.249

Table 2. Exact masses and assignments of fragment ions detected in the LID and CID spectra of protonated RPK $[M+H]^+$ (Figure 3). Error = (*m/z* theoretical – *m/z* experimental)/(*m/z* theoretical)

Assignment	Elemental composition	Theoretical *m/z*	LID		CID	
			Experimental *m/z*	Error (ppm)	Experimental *m/z*	Error (ppm)
$[M+H]^+$	$C_{17}H_{34}O_4N_7$	400.2667	400.2665	-0.500	400.2663	-0.999
$[M+H-H_2O]^+$	$C_{17}H_{32}O_3N_7$	382.2561	382.2564	0.785	382.256	-0.262
$[M+H-2H_2O]^+$	$C_{17}H_{30}O_2N_7$	364.2455	364.2457	0.549	364.2457	0.549
$[M+H-C_3H_7O]^+$	$C_{14}H_{27}O_3N_7$	341.2170	341.2168	-0.586	341.2173	0.879
$(b_2)^+$	$C_{11}H_{20}O_2N_5$	254.1612	254.1610	-0.787	254.1609	-1.180
$(y_2)^+$	$C_{11}H_{22}O_3N_3$	244.1656	244.1654	-0.819	244.1653	-1.229
$(y_2\text{-}2)^+$	$C_{11}H_{20}O_3N_3$	242.1499	242.1502	1.239	ND	NA
$(a_2)^+$	$C_{10}H_{20}ON_5$	226.1662	226.1660	-0.884	226.1660	-0.884
$(x_1)^+$	$C_6H_{13}O_2N_4$	173.0921	173.0924	1.733	ND	NA
$(b_1+2)^+$	$C_6H_{15}ON_4$	159.1240	159.1238	-1.257	ND	NA
$(b_1)^+$	$C_6H_{13}ON_4$	157.1084	157.1082	-1.273	157.1081	-1.910
$(y_1)^+$	$C_6H_{15}O_2N_2$	147.1128	147.1129	0.680	147.1130	1.360
$(a_1+2)^+$	$C_5H_{15}N_4$	131.1291	131.1293	1.525	ND	NA
$(a_1)^+$	$C_5H_{13}N_4$	129.1135	129.1133	-1.549	129.1133	-1.549
$[P]^+$	C_4H_8N	70.0651	70.0652	1.427	70.0650	-1.427

Table 3. Exact masses and assignments of fragment ions detected in the LID spectrum of singly-charged deuterated RPK $[M+D]^+$ (Figure 6). Error = (*m/z* theoretical – *m/z* experimental)/(*m/z* theoretical)

Assignment	**Elemental composition**	**Theoretical *m/z***	**Experimental *m/z***	**Error (ppm)**
$[M+D]^+$	$C_{17}H_{23}D_{11}O_4N_7$	411.3357	411.3356	-0.244
$[M+D-D_2O]^+$	$C_{17}H_{23}D_9O_3N_7$	391.3126	391.3123	-0.769
$[M+D-2D_2O]^+$	$C_{17}H_{23}D_7O_2N_7$	371.2895	371.2892	-0.810
d_6-$(b_2)^+$	$C_{11}H_{14}D_6O_2N_5$	260.1988	260.1986	-0.769
d_5-$(y_2)^+$	$C_{11}H_{17}D_5O_3N_3$	249.1969	249.1965	-1.612
d_5-$(y_2-2)^+$	$C_{11}H_{15}D_5O_3N_3$	247.1813	247.1812	-0.406
d_7-$(a_2)^+$	$C_{10}H_{13}D_7ON_5$	233.2102	233.2098	-1.723
d_4-$(x_1)^+$	$C_6H_9D_4O_2N_4$	177.1284	177.1287	1.703
d_8-$(b_1+2)^+$	$C_6H_7D_8ON_4$	167.1743	167.1741	-1.204
d_6-$(b_1)^+$	$C_6H_7D_6ON_4$	163.146	163.1458	-1.226
d_5-$(y_1)^+$	$C_6H_{10}D_5O_2N_2$	152.1442	152.1439	-1.985
d_7-$(a_1+2)^+$	$C_5H_8D_7N_4$	138.1731	138.1729	-1.447
d_6-$(a_1)^+$	$C_5H_7D_6N_4$	135.1511	135.1509	-1.491
$[P]^+$	C_4H_8N	70.0651	70.0652	1.427

Figure 1. Schematic of the LID experimental set-up in the Q-Exactive mass spectrometer.

Figure 2. a) LID spectrum of the doubly-protonated Bradykinin $[M+2H]^{2+}$ ion (*m/z* 530.79) at 213 nm for 1000 ms (Collision energy 2 eV). b) CID spectrum of doubly-protonated Bradykinin $[M+2H]^{2+}$ ion (*m/z* 530.79) under a normalized CID collision energy of 25 % for 3 ms.

Figure 3. a) LID spectrum of protonated RPK $[M+H]^{+}$ ion (*m/z* 400.27) at 213 nm for 1000 ms (Collision energy 2 eV). b) CID spectrum of protonated RPK $[M+H]^{+}$ ion (*m/z* 400.27) under a normalized CID collision energy of 25 % for 3 ms.

Figure 4. a) Calculated spectrum for the lowest energy structure of protonated RPK $[M+H]^{+}$ ion, using the semi-empirical OM2 method at T=0 K. b) Calculated thermally-broadened absorption spectrum at 300 K.

Figure 5. Snapshots of the non-adiabatic MD "on the fly" using OM2 starting in the second electronic excited state S_2 from the selected trajectory at 300 K of protonated RPK $[M+H]^{+}$ ion. Evidence of a) C-N, b) C-C in proline, and c) C-C in Arginine bond breaking and proton transfer in the first excited state (S_1) during the fragmentation process. Dominant excitations of molecular orbitals in the S_1 state at the time of bond breaking are also shown. a) Fragmentation of C-N bond at 82 fs is characterized by excitation from non-bonding HOMO to non-bonding LUMO localized at C and N atoms, respectively. b) At 18 fs, the C-C bond in proline is breaking, which is characterized by excitation from bonding HOMO to non-bonding LUMO. Trajectory c) shows C-C bond breaking in Arginine at 30 fs and subsequent proton transfer at 74 fs. C-C bond breaking is characterized by excitation to two antibonding MOs.

Figure 6. LID spectrum of singly-charged d_{11}-RPK $[M+D]^{+}$ ion (*m/z* 411.34) at 213 nm for 1000 ms (Collision energy 2 eV) after H/D exchange.

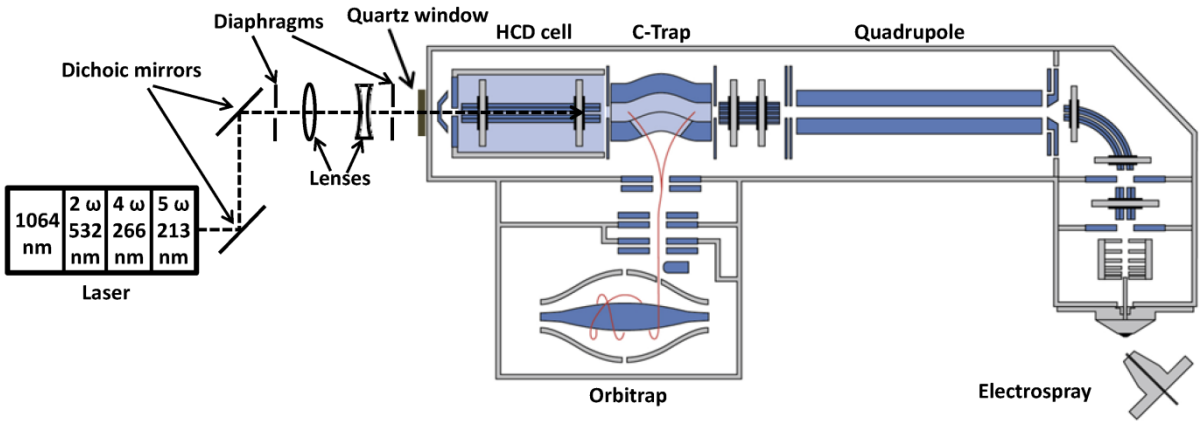

Figure1

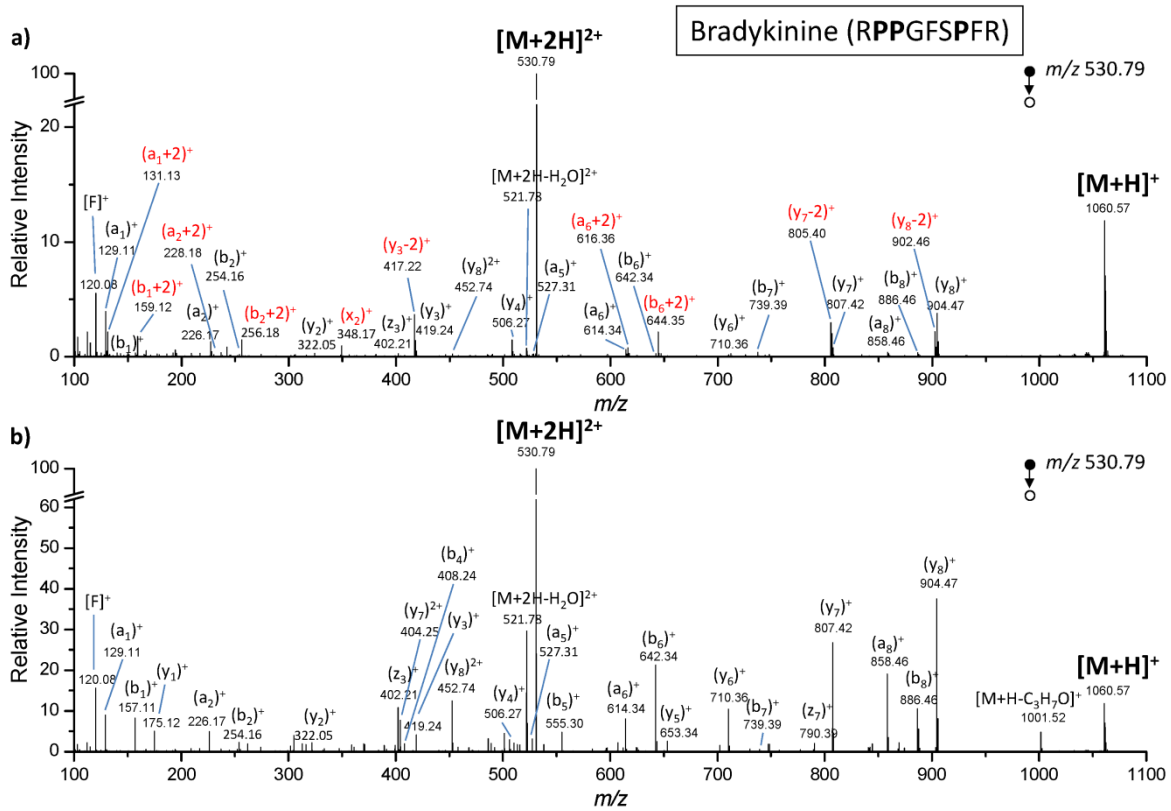

Figure2

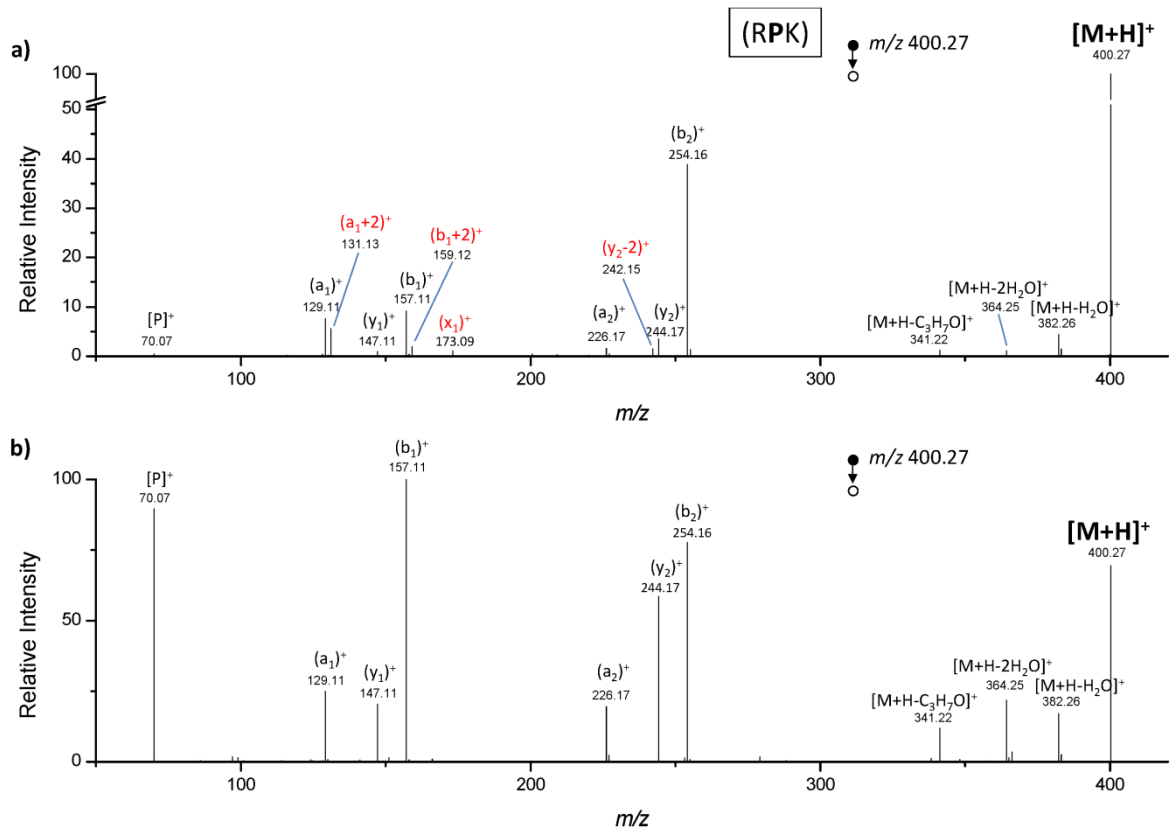
a)
(RPK)
m/z 400.27
[M+H]+
400.27
Relative Intensity
m/z
[P]+
70.07
(a1)+
129.11
(a1+2)+
131.13
(y1)+
147.11
(b1)+
157.11
(b1+2)+
159.12
(x1)+
173.09
(a2)+
226.17
(y2-2)+
242.15
(y2)+
244.17
(b2)+
254.16
[M+H-C3H7O]+
341.22
[M+H-2H2O]+
364.25
[M+H-H2O]+
382.26
b)
m/z 400.27
[M+H]+
400.27

Figure3

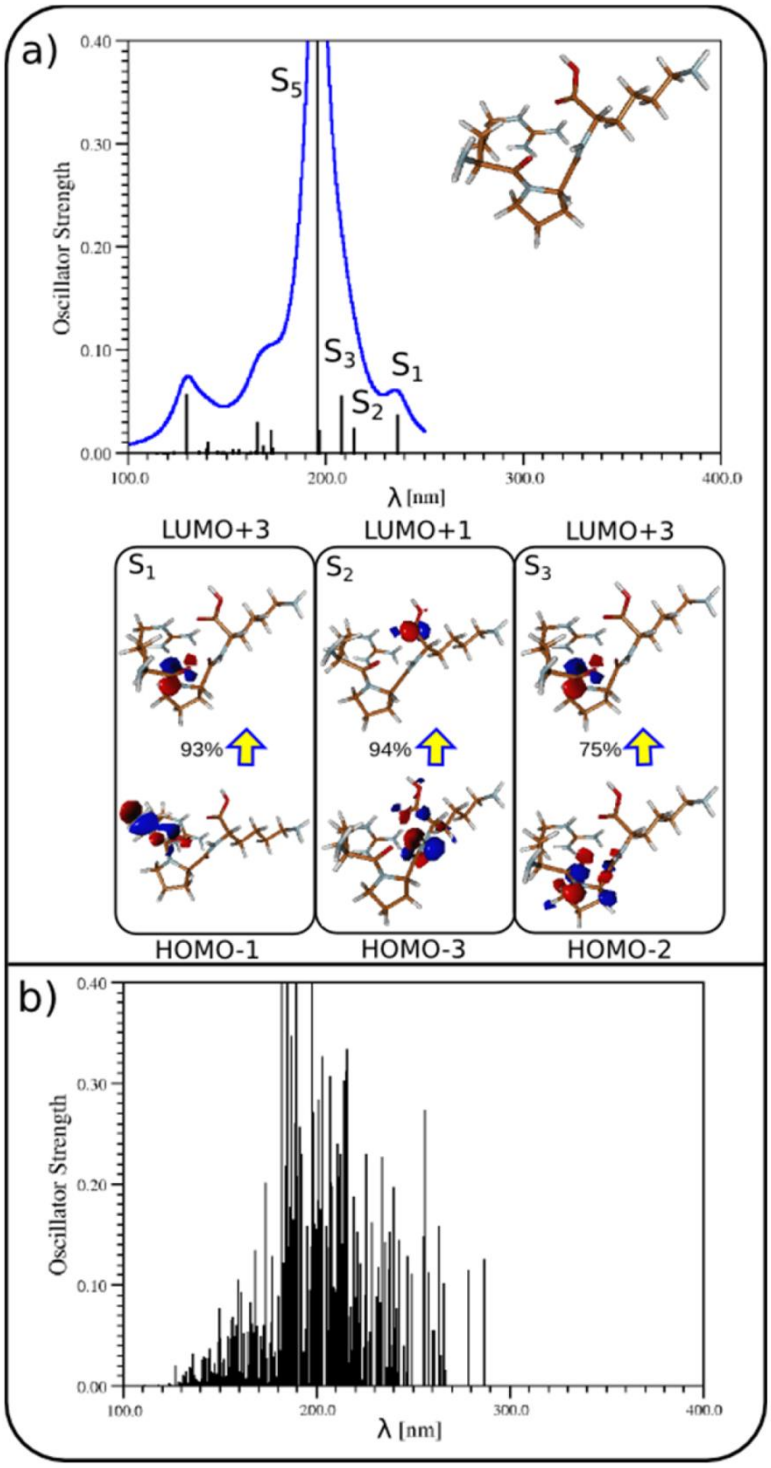
a)
Oscillator Strength
λ [nm]
S5
S3
S1
S2
LUMO+3
LUMO+1
LUMO+3
S1
S2
S3
93%
94%
75%
HOMO-1
HOMO-3
HOMO-2
b)
Oscillator Strength
λ [nm]

Figure4

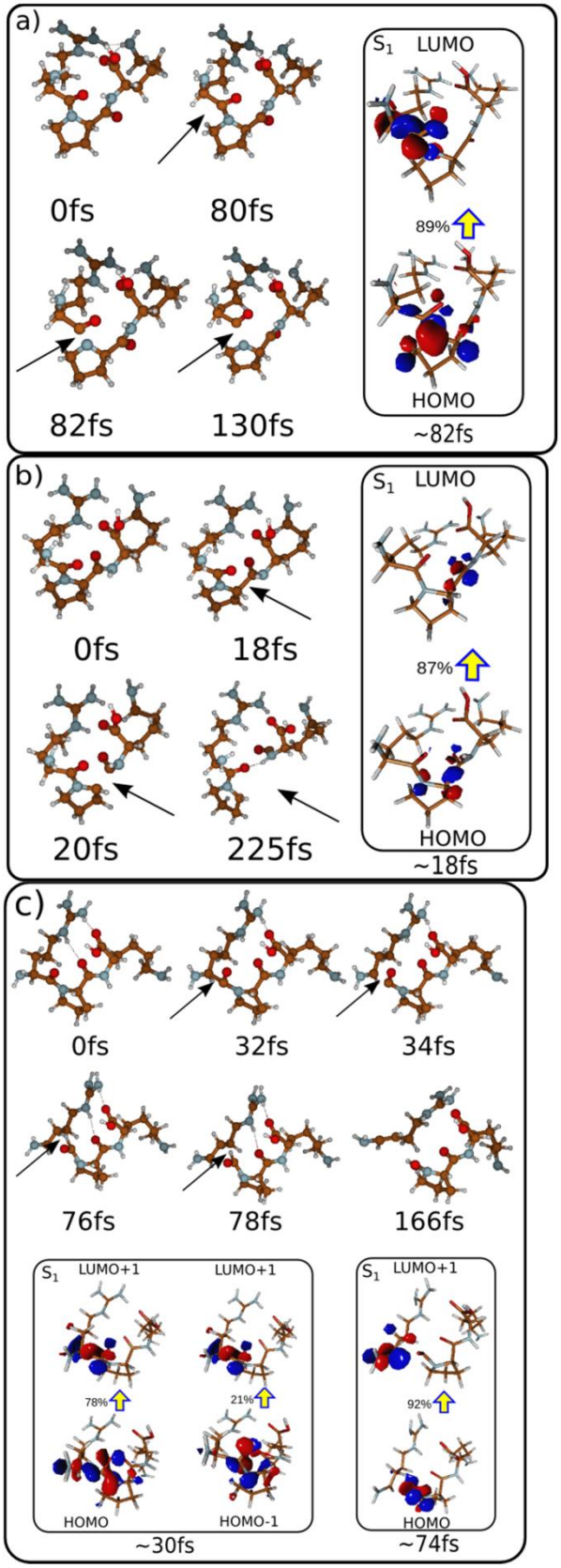
a)
0fs
80fs
82fs
130fs
S1 LUMO
89%
HOMO
~82fs
b)
0fs
18fs
20fs
225fs
S1 LUMO
87%
HOMO
~18fs
c)
0fs
32fs
34fs
76fs
78fs
166fs
S1 LUMO+1
LUMO+1
78%
21%
HOMO
HOMO-1
~30fs
S1 LUMO+1
92%
HOMO
~74fs

Figure5

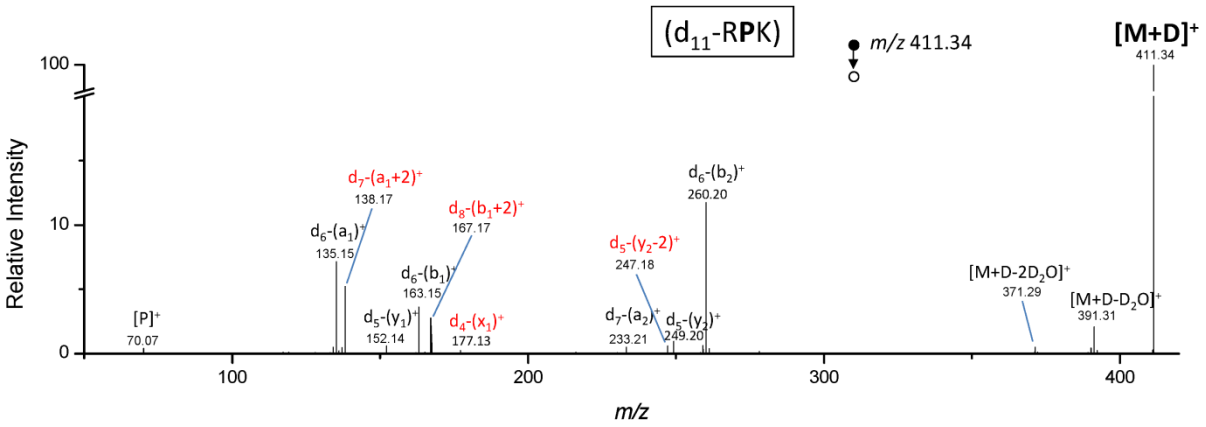
(d11-RPK)
m/z 411.34
[M+D]+
411.34
Relative Intensity
100
10
0
d7-(a1+2)+
138.17
d8-(b1+2)+
167.17
d6-(a1)+
135.15
d6-(b1)+
163.15
d5-(y1)+
152.14
d4-(x1)+
177.13
[P]+
70.07
d6-(b2)+
260.20
d5-(y2-2)+
247.18
d7-(a2)+
233.21
d5-(y2)+
249.20
[M+D-2D2O]+
371.29
[M+D-D2O]+
391.31
100
200
300
400
m/z

Figure6

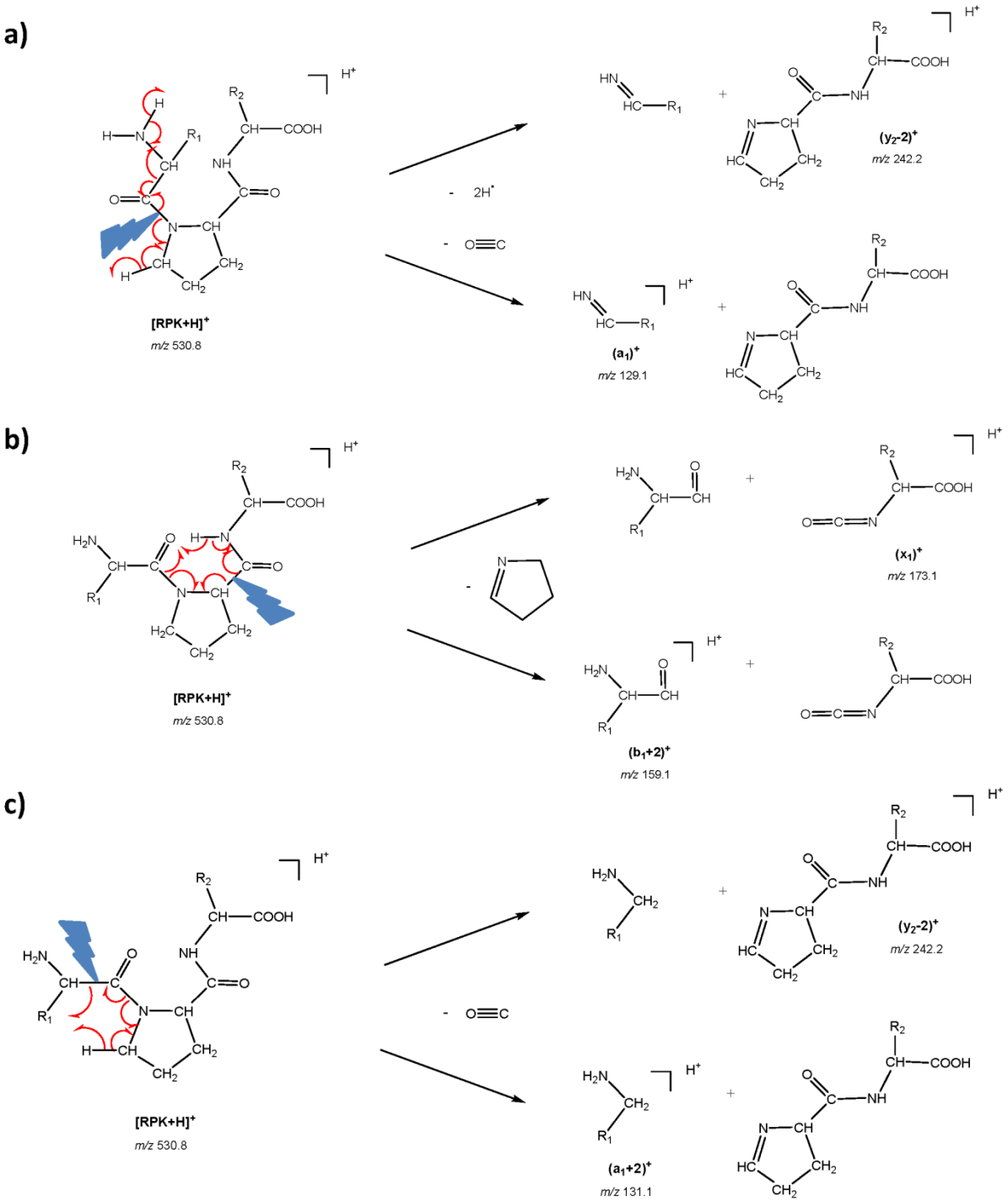
a)
[RPK+H]+
m/z 530.8
- 2H•
- O≡C
(y2-2)+
m/z 242.2
(a1)+
m/z 129.1
b)
[RPK+H]+
m/z 530.8
(x1)+
m/z 173.1
(b1+2)+
m/z 159.1
c)
[RPK+H]+
m/z 530.8
(y2-2)+
m/z 242.2
(a1+2)+
m/z 131.1

Scheme1

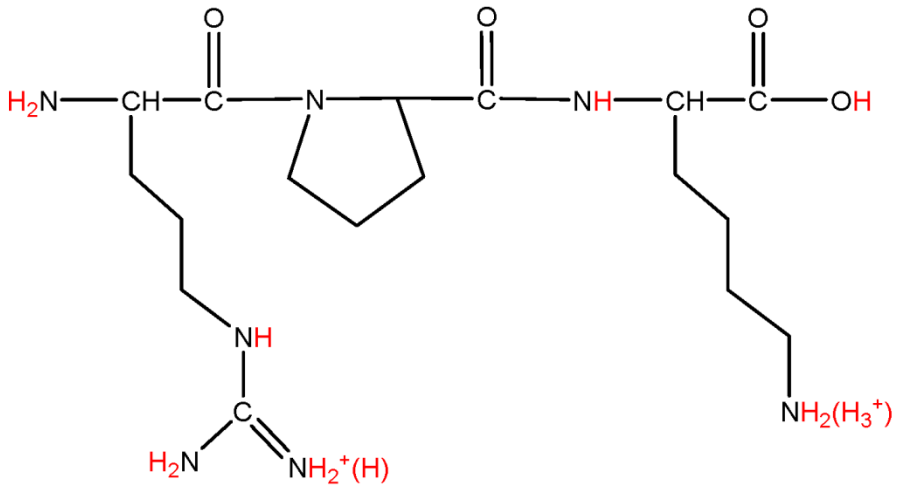

Scheme2